Cogeneration System of Power, Cooling, and Hydrogen from Geothermal Energy: An Exergy Approach

Nourozi, Nima
Department of Energy Engineering and Physics, Amirkabir University of Technology (Tehran Polytechnic), Tehran, I.R. IRAN

Ebadi, Abdol Ghaffar
Department of Agriculture, Jouybar Branch, Islamic Azad University, Jouybar, I.R. IRAN

Bozorgian, Alireza*[+]
Department of Chemical Engineering, Mahshahr Branch, Islamic Azad University, Mahshahr, I.R. IRAN

Hoseyni, Seyed Jalal
Department of Chemistry, Shams Gonbad Higher Education Institute, Gonbad Kavous, I.R. IRAN

Vessally, Esmail
Department of Chemistry, Payame Noor University, Tehran, I.R. IRAN

ABSTRACT: *Production systems have experienced rapid growth over the past few years. Based on geothermal energy, the present study explores a unique cogeneration system that includes a proton membrane electrolyzer, the Rankine cycle, and a water-ammonia absorption chiller. The model under study is designed to generate power and hydrogen, as well as cooling, and it is analyzed from an energy and exergy standpoint. For the desuperheater and the absorber, the maximum rate of exergy destruction of the Rankin cycle is 34% and 36%, respectively. Furthermore, a parametric analysis of the system was conducted, and the cogeneration system was optimized from three perspectives: turbine production power, energy efficiency, and exergy. Based on turbine inlet and outlet pressure, turbine power, energy efficiency, and system efficiency are optimized. Moreover, the optimization calculations made from the perspective of turbine production power show that production power values are 101 kW, hydrogen production is 4.24 liters per second, system energy efficiency is 82.3%, and the amount of heat absorbed in the evaporator is 57.6 kW.*

KEYWORDS: *Exergy analysis; Cogeneration; Hydrogen production; Absorption chiller; Geothermal Energy.*

***** *To whom correspondence should be addressed.*
+ *E-mail*: *a.bozorgian@mhriau.ac.ir*
1021-9986/2022/2/706-721 *16/$/6.06*

INTRODUCTION

Fossil fuel resources are declining around the world, and their overuse has had environmental consequences. Today, the main goal of most countries is to find new energy sources and renewable energy. It is predicted that the amount of energy produced in the world through renewable energy will triple from 2010 to 2035 and will reach 31% of the total energy produced worldwide [1]. Geothermal energy is one of the renewable energy sources that have many benefits. The advantages of geothermal energy are the absence of environmental pollutants and its high capacity for power generation [2, 3]. The temperature of geothermal energy sources varies between 50 and 350 degrees Celsius. Due to the existence of many low-temperature sources (90 to 220 degrees Celsius) in the world, it is predicted that these sources will be used more in the future [4]. On the other hand, organic Rankin cycles are the most suitable cycles for geothermal energy [5-7]. Therefore, optimizing and improving the performance of organic Rankine cycles seems necessary. Hydrogen is one of the types of clean energy, and only water is produced from its combustion [8, 9]. Also, various types of renewable energy such as solar, wind, and geothermal can produce it [10-12]. In recent years, the use of proton converter membranes to produce hydrogen has become very popular due to the production of purer hydrogen and the possibility of using renewable energy [13]. Researchers have done much research to improve the efficiency of geothermal cycles. Ratlamwala and Dincer [14] investigated a simultaneous generation of power and hydrogen-based on the geothermal energy of a multiple evaporation cycle. According to the obtained results, the exergy efficiency has increased from 6.53% to 47.29% by increasing the number of evaporation stages from one stage to five stages. *Cao et al.* [15] examined seven different arrangements of geothermal and hydrogen production by electrolysis. Their calculations showed a reduction in the cost of hydrogen production in exchange for an increase in the temperature of the geothermal source. Atalay [16] used geothermal energy to produce hydrogen and fresh water and achieved a return on investment of 5.6 years. *Norouzi et al*. [17] analyzed a system of cogeneration of power, hydrogen, and cooling with solar energy. Based on the results of their research, the amount of thermal efficiency was 34.98%, and exergy efficiency was 49.17%. *Yuksel et al.* [18] also examined a system of cogeneration of power, hydrogen, and cooling and presented that by increasing the temperature of the hot source from 130 to 200 ° C, the amount of hydrogen produced from 0.03 to 0.075 kg Increases per second. *Norouzi et al.* [19] studied a system of simultaneous generation of power, heating, and hydrogen on nuclear energy. Based on the results of their work, the amount of thermal efficiency, exergy efficiency, and total unit cost of production in the optimal state were 94.84%, 47.89%, and $ 89.95 per gigajoule, respectively. *Balta et al.* [20] studied a combined system of geothermal and thermochemical water separation cycles and investigated the amount of hydrogen produced. The results of their thermodynamic analysis showed that the cost of hydrogen production is directly dependent on the capacity of the plant and the exergy efficiency. *Cai et al.* [21] examined the optimal methods of producing hydrogen by electrolysis using renewable energy sources and compared their effectiveness. *Ovalie et al.* [22] conducted a study on the utilization of hydrogen sulfide to produce hydrogen using geothermal energy sources. *Mahmoud et al.* [23] present a review of hydrogen production systems using geothermal energy, showing the importance and potential of this technology in addition to the main obstacles facing this domain. The effect of several parameters was taken into consideration, such as geothermal fluid temperature, water electrolysis temperature, working fluid, and type of power cycle. The different types of geothermal power plants were also compared, namely, flash, binary, flash-binary, recuperative, regenerative, and organic Rankine flash cycles. This study covers a wide range of investigations regarding hydrogen production rate, hydrogen production cost, energetic efficiency, exergetic efficiency, exergetic cost, and electricity generated. A work by Parham and Assadi [24] is an attempt to propose and analyze a geothermal-based multi-generation system. The proposed cogeneration system consists of different sections, namely: organic Rankine cycle, geothermal wells, absorption heat transformer, domestic water heater, and proton exchange membrane electrolyzer. To assess the cycle's performance, thermodynamic models were developed and a parametric study was carried out. For this purpose, energetic analyses are undertaken on the proposed system. Also, the effects of some important variables such as geothermal water temperature, turbine inlet temperature, and pressure on several parameters such as energy efficiencies

of the proposed system, water production, net electrical output power, and hydrogen production are investigated. It is shown that, by boosting geothermal water temperate, COP of the AHT increases and flow ratio decreases. Additionally, increasing absorber temperature leads to the reduction of the energy utilization factor. A work by *Han et al.* [25] proposes a thermodynamic analysis and optimization of a flash-binary geothermal cycle for power generation and hydrogen production aims where the binary cycle used is an organic Rankine cycle in which different mixtures of zeotropic fluids are used as the working fluid. The integration of ORC and zeotropic mixtures presents the considerable capability to combine their superiority and further enhance the system performance considerably. The superiority of the proposed system which combines the advantages of zeotropic mixtures with ORC positive aspects is revealed through the energy and exergy analysis. *Yuksel et al.* [26] propose an integrated system aiming for hydrogen production with by-products using geothermal power as a renewable energy source. In analyzing the system, an extensive thermodynamic model of the proposed system is developed and presented accordingly. In addition, the energetic and exergetic efficiencies and exergy destruction rates for the whole system and its parts are defined. Due to the significance of some parameters, the impacts of varying working conditions are also investigated. The results of the energetic and exergetic analyses of the integrated system show that the energy and exergy efficiencies are 39.46% and 44.27%, respectively. Furthermore, the system performance increases with the increasing geothermal source temperature and reference temperature while it decreases with the increasing pinch point temperature and turbine inlet pressure. A study by *Cao et al.* [27] uses the total capacity of a medium-temperature geothermal source to produce energy-based products and eliminate the weakness of the conventional setups, increasing the exergy and exergoeconomic performances. A parametric study has been implemented to analyze the effect of several main parameters on the vital variables including efficiencies, exergy destruction rate, sum unit exergy cost, investment cost rate, and exergoeconomic factor. Besides, multi-objective optimization in different cases has been applied to the calculations through a non-dominated sorting genetic algorithm II (NSGA-II) to achieve an optimal design. The results showed that the performance of the system was more sensitive to changing the separators' operating pressure of the plant. Likewise, the optimum exergy efficiency and optimum unit exergy cost of the system were found to be 12% and 0.0043 $/kWh through the exergy/cost multi-objective optimization case, correspondingly. A paper by *Cao et al.* [28] investigates a combined cooling and power system driven by geothermal energy for ice-making and hydrogen production. The proposed system combines the geothermal flash cycle, Kalina cycle, ammonia-water absorption refrigeration cycle, and the electrolyzer. Geothermal energy can be efficiently converted to storable hydrogen and ice. Based on the mathematical model, some key parameters are analyzed to figure out their effect on the exergetic performance. An exergy destruction analysis for all components has been performed to find out the distribution of exergy inefficiency. The system exergetic efficiency is optimized by Jaya algorithm and Genetic algorithm and the optimization results are compared. According to the parametric analysis, the exergy efficiency decreases as the back pressure of the steam turbine and the back pressure of the ammonia-water turbine increase. The exergy efficiency could increase first and then decline, as flash pressure, ammonia-water turbine inlet pressure, and ammonia mass fraction of basic solution increase. In a study by *Yilmaz et al.* [29] the thermodynamic and economic analysis of geothermal energy-assisted hydrogen production system was performed using real-time Artificial Neural Networks on Field Programmable Gate Array. During the modeling of the system in the computer environment, a liquid geothermal resource with a temperature of 200 °C and a flow rate of 100 kg/s was used for electricity generation, and this electricity was used as a work input in the electrolysis unit to split off water into the hydrogen and oxygen.

Results of previous studies show that multigeneration systems have shown great potential to enhance the overall system's efficiency, leading to reduced production costs. The integration of another energy source was found to be interesting in geothermal-driven hydrogen production systems. This would promote the adoption of a multigeneration system as well as increase the geothermal fluid's temperature before entering the power cycle. Previous research has examined hydrogen production and adsorption cooling with an organic Rankine base cycle. To achieve higher hydrogen content and more refrigeration capacity and increase cycle efficiency, this research uses

the modified organic Rankin cycle, which uses the maximum available heat sources. The main purpose of this study is to use geothermal energy as a source of low-temperature energy for a new organic rank cycle to cogenerate power, cooling, and hydrogen Also, regarding the previous works, it found that many researchers have examined geothermal pumps, and it is remarkable that there are few types of research which have analyzed the direct use of geothermal wells for cogeneration goals. In this research, a new cogeneration cycle to produce power, hydrogen, oxygen, and heating from geothermal wells were investigated. This cogeneration cycle includes a new configuration, PEM, and domestic cooling system. The purposes of this study are multifold and the use of different geothermal wells as the energy source for the cogeneration cycle to produce power, heating, cooling, and hydrogen; A comprehensive parametric study to investigate the effect of parameters on the performance of the cycle; Optimization of the cogeneration cycle and ORC. Investigating the amount of hydrogen and cooling produced, the effect of using two different operating fluids (Water + ammonia and R134a), and the use of different heat exchanger arrangements to achieve maximum heat source use are among the innovations of this study.

EXPERIMENTAL SECTION

Description of the system

The present study combines a proton membrane electrolyzer system and a water and ammonia absorption refrigeration system with an organic Rankine cycle. Geothermal energy has been used to power the Rankin-Eli cycle. Fig. 1 shows the cycle under consideration, including a system for the simultaneous generation of power, hydrogen, and cooling with a geothermal energy source. This system consists of four subsystems. Organic Rankine cycle subsystem, geothermal subsystem, absorption cooling subsystem, and hydrogen production subsystem. The main output of this system is power, hydrogen, and refrigeration, which are produced under the organic Rankine cycle system, hydrogen and cooling, respectively. The geothermal subsystem supplies the main energy of the system. The operating fluid of this cycle, according to previous research, is R134a[15], which is first pumped to a recycled heat exchanger and preheated by recycled heat, and then superheated by geothermal heat exchangers to the maximum cycle temperature. This heat exchanger consists of an economizer, an evaporator, and a superheater. The fluid is first preheated by the recycled heat, enters the economizer, then converted to saturated steam in the evaporator, and finally in the superheater from saturated steam to superheated steam. The superheated fluid then enters the turbine and produces work in a real process. After passing through the turbine and generating power, the operating fluid is still capable of generating heat, and its heat can be used to provide the necessary heat for the absorption refrigeration cycle. Therefore, it enters the de-superheater and supplies the necessary energy to the absorption chiller generator. The operating fluid then enters the condenser and is converted to a saturated liquid by dissipating heat and producing the hot water needed for the hydrogen production subsystem, and so on.

The power generated by the organic Rankine cycle in a generator is converted to electrical energy and transferred entirely to the proton membrane system to produce hydrogen.

In the electrolyzer system, as shown in Fig. 1, the inlet water enters the condenser heat exchanger at atmospheric pressure and is heated to the required temperature for the electrolyzer system. In an electrolyzer system, the hydrogen leaving the cathode dissipates its heat to the environment and is stored in a source. The oxygen produced at the anode is separated from the mixture of water and oxygen by a separator, and finally, the remaining water is returned to the electrolyzer to produce hydrogen.

The heat dissipated in the superheater enters the generator of an absorption refrigeration system. There, the steam is separated from the refrigerant, and the refrigerant steam goes to the evaporator after passing through the condenser and changing phase to liquid. In the evaporator part, absorbing heat from the pipes inside the evaporator causes cooling and reduces the temperature of the fluid. The liquid separated in the generator, called a concentrated solution enters the absorber to absorb the refrigerant vapor. Two heat exchangers have been used to increase heat exchange and system efficiency.

Geothermal water in a saturated liquid state first enters the superheater and then enters the evaporator and economizer, and with heat exchange and energy transfer, the temperature decreases and returns to earth. To simplify the equations, the following hypotheses have been used [23].

• All cycle components operate in a steady state.

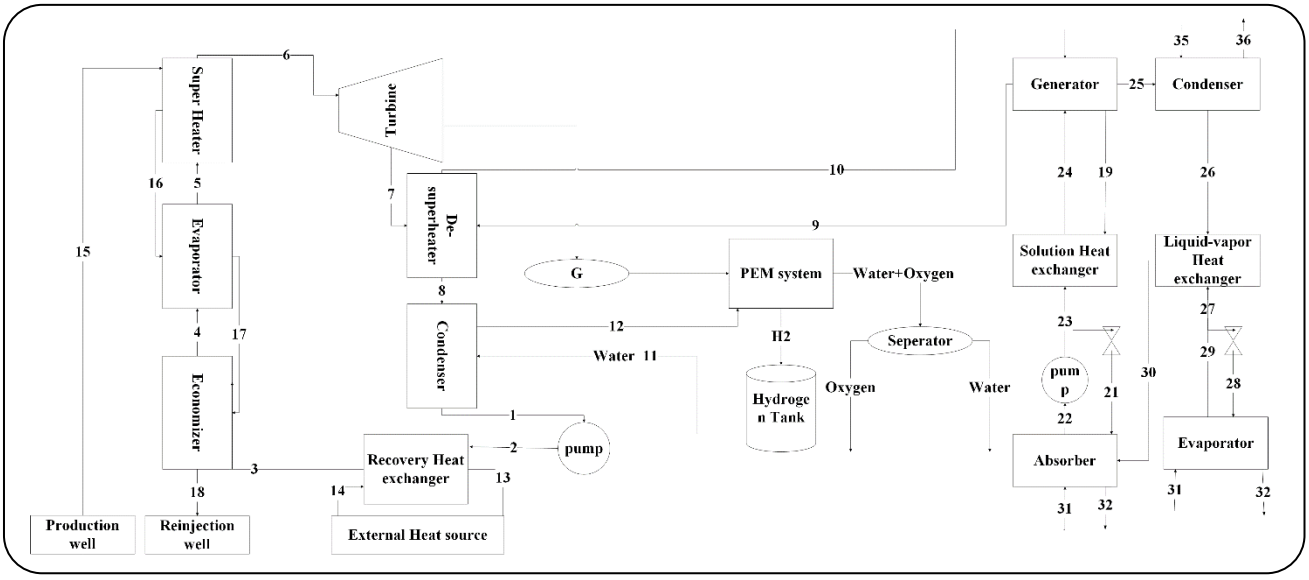

Fig. 1: Proposed model of the system for cogeneration of power, hydrogen, and cooling.

• Pressure drops of pipes, heat exchangers, and other components are omitted.

• water is used in the geothermal cycle and the R134a is used in the ORC unit.

• Ambient temperature and pressure are equal to 25 °C and 100 kPa, respectively.

• The geothermal water temperature is assumed to be 169°C, and its flow rate is 1 kg/s[23].

• The whole adiabatic system is considered, and heat loss is eliminated.

The input data for the organic Rankine cycle, the adsorption refrigeration system, and the proton membrane electrolyzer system are given in Table 1.

Energy analysis and exergy

To model, the system's energy, mass, and energy conservation rules must be applied to each component of the system. For this purpose, each element is considered as a control volume [24].

$$\sum_i \dot{m}_i = \sum_e \dot{m}_e \quad (1)$$

$$\dot{Q} - \dot{W} = \sum_e \dot{m}_e h_e - \sum_i \dot{m}_i h_i \quad (2)$$

Exergy [24] is divided into physical exergy, chemical exergy, kinetic exergy, and potential exergy. Due to small changes in speed and altitude, and changes in the chemical composition of flows, the terms of kinetic, potential, and chemical exergy have been omitted in this study (chemical exergy is only considered during the fuel cell process). Physical exergy is considered the maximum useful work of the theory obtained by the system in interaction with the environment in equilibrium conditions [25]. Considering the first and second laws of thermodynamics, the exergy balance can be considered as follows.

$$\dot{Ex}_Q + \sum_i \dot{m}_i ex_i = \sum_e \dot{m}_e ex_e + \dot{Ex}_W + \dot{Ex}_D \quad (3)$$

Indices i and e specify the input and output exergy to the control volume. Ex_D represents exergy destruction, and the other terms are determined by Equations (4-6).

$$\dot{Ex}_Q = (1 - \frac{T_0}{T_i})\dot{Q}_i \quad (4)$$

$$\dot{Ex}_W = \dot{W} \quad (5)$$

$$ex = ex_{ph} = (h - h_0) - T_0(s - s_0) \quad (6)$$

The energy efficiency of the cogeneration system under consideration is calculated based on Eq. (7)[25-29].

$$\eta_{th} = \frac{\dot{W}_{net} + \dot{Q}_{heating}}{\dot{Q}_{Recovery} + \dot{Q}_{Geothermal}} \quad (7)$$

$$\dot{Q}_{brine} = \dot{m}_9(h_{10} - h_9) + \dot{m}_{11}(h_{12} - h_{11}) \quad (8)$$

$$W_{net} = W_{turbine} - W_{pumps} \quad (9)$$

The exergy efficiency of the cogeneration system is obtained based on Eq. (10)[30].

$$\eta_{ex} = 1 - \left(\frac{Ex_{D,tot}}{Ex_{QGeothermal} + Ex_{Recovery}}\right) \quad (10)$$

Table 1: Organic Rankin cycle input data [15].

Parameter			Value
Isentropic turbine efficiency (%)			80
Isentropic pump efficiency (%)			80
Inlet pressure to the turbine (kPa)			3800
Turbine outlet pressure (kPa)			1150
Pinch Superheater temperature difference (ºC)			5
Condenser pinch temperature difference (ºC)			5
Condenser inlet water pressure (kPa)			100
Inlet water flow to the superheater (kg/s)			1.1
Solar Converter Pinch Temperature Difference (ºC)			10
Evaporator pinch temperature difference (ºC)			5
Super Heater Pinch Temperature Difference (ºC)			10
Absorption refrigeration cycle input data			
Condenser inlet water temperature (ºC)			30
Condenser outlet water temperature (ºC)			35
Evaporator inlet water temperature (ºC)			7
Evaporator outlet water temperature (ºC)			12
Heat exchanger efficiency (%)			90
Pump efficiency (%)			80
Condenser, evaporator, and absorber water pressure (kPa)			100
Generator inlet water pressure (kPa)			200
Proton membrane electrolyzer input data [20]			
Parameter	value	Parameter	Value
Po (bar)	1	T_{PEM} (ºC)	76
D (mm)	50	$E_{act,a}$ (kJ/mole)	18
F (C/mol)	96486	$E_{act,c}$ (kJ/mole)	14
J_a^{ref} (A/m^2)	170000	λ_a	10
J_c^{ref} (A/m^2)	4600	λ_c	80

Tables 2 and 3 present the Rankine cycle exergy equations and the absorption cycle[31-34].

The electrolyzer relationships are presented in Table 4.

To solve the system, first energy analysis and then exergy analysis is performed for it. EES software has been used to solve thermodynamic equations.

Optimization

In the proposed cogeneration system, the turbine output power, the heat generated in the condenser, and the cogeneration system's efficiency depend on the pressures before and after the turbine (P6 and P7). These two states shows are effective on the electricity generated in this system and both can be analyzed to estimate the most suitable turbine configuration and throttle pressure. In this paper, three different optimal functions are defined and optimized for two variables. Optimization is done using the genetic algorithm method and EES software. This algorithm was first introduced by John Hand. The genetic algorithm is based on the gradual evolution of living things [34-37].

Table 2: Exergy rates of fuel and Rankine cycle product.

Component name	Fuel Exergy	Product Exergy
Turbine	$\dot{E}_6 - \dot{E}_7$	$\dot{W}_{tur}$
Superheater	$\dot{E}_7 - \dot{E}_8$	$\dot{E}_{10} - \dot{E}_9$
Condenser	$\dot{E}_8 - \dot{E}_1$	$\dot{E}_{12} - \dot{E}_{11}$
Pump	$\dot{W}_{pump}$	$\dot{E}_2 - \dot{E}_1$
Recovery heat exchanger	$\dot{E}_{14} - \dot{E}_{13}$	$\dot{E}_3 - \dot{E}_2$
Economizer	$\dot{E}_{17} - \dot{E}_{18}$	$\dot{E}_4 - \dot{E}_3$
Evaporator	$\dot{E}_{16} - \dot{E}_{17}$	$\dot{E}_5 - \dot{E}_4$
Super Heater	$\dot{E}_{15} - \dot{E}_{16}$	$\dot{E}_6 - \dot{E}_5$

Table 3: Exergy rates of fuel and absorption cycle product.

Component name	Fuel Exergy	Product Exergy
Condenser	$\dot{E}_{25} - \dot{E}_{26}$	$\dot{E}_{36} - \dot{E}_{35}$
Liquid-steam heat exchanger	$\dot{E}_{26} - \dot{E}_{27}$	$\dot{E}_{30} - \dot{E}_{29}$
Expansion valve	$\dot{E}_{27}$	$\dot{E}_{28}$
Evaporator	$\dot{E}_{28} - \dot{E}_{29}$	$\dot{E}_{34} - \dot{E}_{33}$
Absorber	$\dot{E}_{30} + \dot{E}_{31} + \dot{E}_{21}$	$\dot{E}_{22} + \dot{E}_{32}$
Pump	$\dot{W}_{pump}$	$\dot{E}_{23} - \dot{E}_{22}$
Soluble heat exchanger	$\dot{E}_{19} - \dot{E}_{20}$	$\dot{E}_{24} - \dot{E}_{23}$
Generator	$\dot{E}_{10} + \dot{E}_{24}$	$\dot{E}_9 + \dot{E}_{19} + \dot{E}_{25}$

Table 4: Relationships of proton membrane electrolyzers [20].

Parameter	Equation
Electrolyzer voltage	$V = V_O + V_{act,c} + V_{act,a} + V_{ohm}$
Electrolyzer power consumption	$E_{electric} = JV, E_{electric} = \dot{W}_{ORCT}$
Cathode activation potential	$V_{act,c} = \frac{RT}{F}\sinh^{-1}\left(\frac{J}{2J_{0,c}}\right)$ $J_{0,c} = \int_c^{ref} \exp\left(\frac{-E_{act,c}}{RT}\right)$
Anode activation potential	$V_{act,a} = \frac{RT}{F}\sinh^{-1}\left(\frac{J}{2J_{0,a}}\right)$ $J_{0,a} = \int_a^{ref} \exp\left(\frac{-E_{act,a}}{RT}\right)$
Ohmic potential	$V_{ohm} = JR_{PEM}$ $R_{PEM} = \int_0^D \frac{dx}{\sigma_{PEM}[\lambda(x)]}$ $\lambda(x) = \frac{\lambda_a - \lambda_c}{D}x + \lambda_c$ $\sigma_{FEM}[\lambda(x)] = [0.5139\lambda(x) - 0.326] \times \exp\left[1268\left(\frac{1}{303} - \frac{1}{T}\right)\right]$
Reversible potential	$V_O = 1.229 - 0.00085(T_{PEM} - 298)$
Molar flow rate of oxygen	$\dot{N}_{H_2,out} = \frac{J}{2F} = \dot{N}_{H_2O,reacted}$
Molar flow rate of oxygen	$\dot{N}_{O_2,out} = \frac{J}{4F}$
Residual water flow rate	$\dot{N}_{H_2O,out} = \dot{N}_{H_2O,in} - \frac{J}{2F}$

Table 5: Range of changes in optimization parameters.

Parameter name	Range	Symbol
Turbine inlet pressure (kPa)	3000-3800	P_6
Turbine outlet pressure (kPa)	500-1150	P_7

**Both the Turbine inlet and outlet can be considered the most important parameters in designing any Rankine system. The turbine inlet is the throttle pressure which significantly impacts the overall performance and configuration of the system and turbine outlet pressure is effective on the condensing system and turbine sizing.*

Table 6: Functional parameters of a cogeneration system (for R134a as operating fluid).

Variable name	Value
Turbine generation capacity (kW)	70.45
Pump power (kW)	7.72
Superheater heat (kW)	118.7
Condenser heat (kW)	494.9
Heat absorbed in the evaporator (kW)	83.5
Hydrogen produced (lit/s)	3.133
Absorption system performance coefficient	0.712
Energy efficiency of cogeneration system	0.740
Exergy efficiency of the cogeneration system	0.651

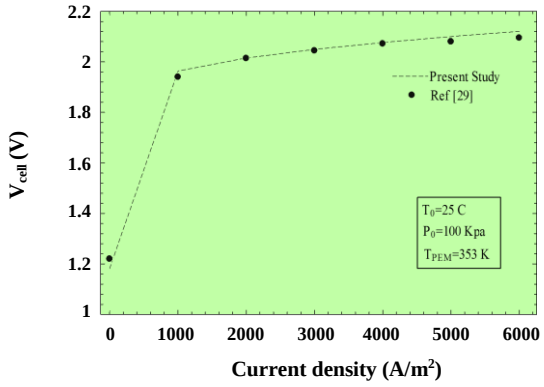

Fig. 3: Hydrogen Production Modeling Results [29].

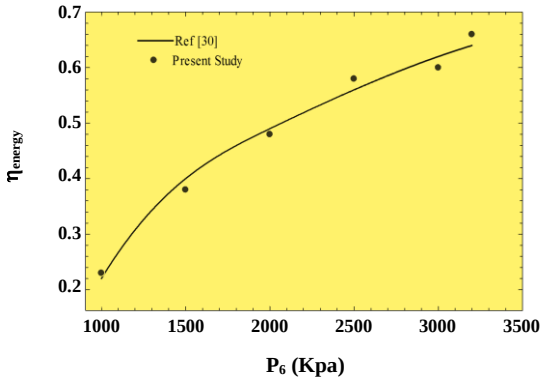

Fig. 4: Organic Rankine Cycle Modeling Results [30].

In the present study, optimization is performed based on the effective parameters (P6 and P7). The range of changes in these parameters is presented in Table 5.

RESULTS AND DISCUSSION

In the first case of the cogeneration system, the pre-turbine pressure values of P7 are 3800 kPa, and the post-turbine pressure is 1150 kPa. The values of system performance parameters are presented in Table 6. For this case, the thermodynamic properties of different points of the organic Rankine cycle and the adsorption refrigeration cycle are presented in Table 7.

Validation

To determine the accuracy of the calculations, the hydrogen production and organic Rankine cycle sections are compared with the results of previous studies, and the results are presented in Figs. 3 and 4, which show a good agreement between the results.

Table 7: Thermodynamic properties of the proposed cycle.

State	s (kJ/kg.k)	h (kJ/kg)	m (kg/s)	P (kPa)	T (°C)	Fluid	State	S (kJ/kg.k)	h (kJ/kg)	m (kg/s)	Xi	T (°C)	Fluid
1	0.417	115.4	2.634	1150	44.66	R134a	19	1.187	198.0	0.294	0.397	95.0	Water + ammonia
2	0.419	118.3	2.634	3800	47.00	R134a	20	0.478	-43.90	0.294	0.397	41.1	Water + ammonia
3	0.634	192.0	2.634	3800	90.04	R134a	21	0.481	-43.90	0.294	0.397	41.3	Water + ammonia
4	0.698	215.5	2.634	3800	97.77	R134a	22	0.366	-82.41	0.365	0.513	35.0	Water + ammonia
5	0.837	267.2	2.634	3800	97.77	R134a	23	0.367	-81.12	0.365	0.513	35.2	Water + ammonia
6	1.112	375.1	2.634	3800	159.0	R134a	24	0.957	113.51	0.365	0.513	74.4	Water + ammonia
7	1.128	348.2	2.634	1150	114.0	R134a	25	4.615	1422	0.073	0.990	74.4	ammonia
8	1.006	303.3	2.634	1150	71.66	R134a	26	0.587	158.2	0.073	0.990	35.0	ammonia
9	1.057	328.2	1.1	200	78.41	Water	27	0.180	37.94	0.073	0.990	9.9	ammonia
10	1.352	435.8	1.1	200	103.8	Water	28	0.186	37.94	0.073	0.990	2.0	ammonia
11	0.225	63.1	2.293	100	15.0	Water	29	4.389	1203	0.073	0.990	7.0	ammonia
12	0.913	279.0	2.293	100	66.67	Water	30	4.812	1323	0.073	0.990	32.1	ammonia
13	5.836	341.9	6	100	68.02	Air	31	0.437	123.9	5.353	-	30.1	Water
14	5.926	374.2	6	100	100.0	Air	32	0.506	146.9	5.353	-	35.0	Water
15	2.032	715.0	1	772.5	169.1	Geo	33	0.181	50.55	3.983	-	12.0	Water
16	1.338	431.2	1	772.5	102.9	Geo	34	0.107	29.76	3.983	-	7.0	Water
17	1.338	431.2	1	772.5	102.9	Geo	35	0.437	125.9	4.33	-	30.0	Water
18	1.169	369.3	1	772.5	88.1	Geo	36	0.506	146.8	4.33	-	35.1	Water

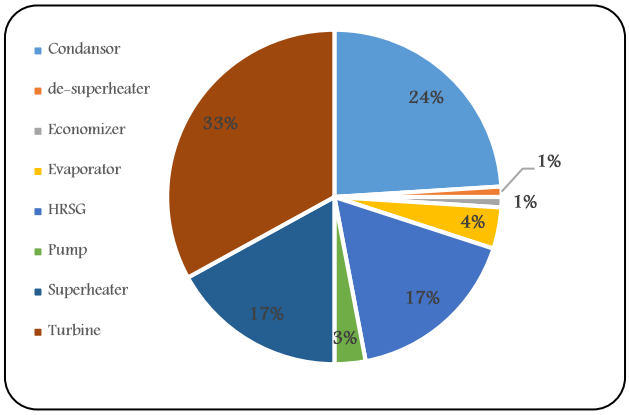

Fig. 4: Exergy destruction of organic Rankine cycle components.

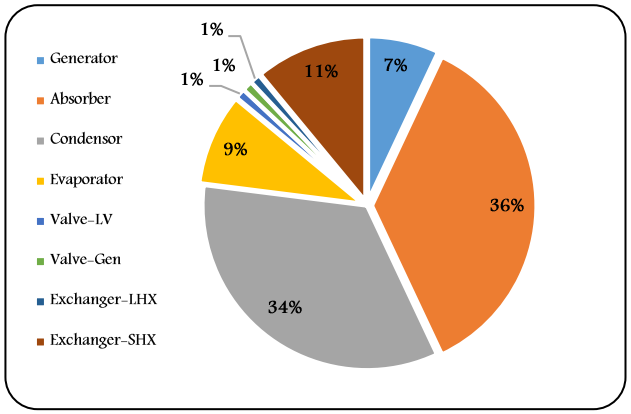

Fig. 5: Exergy destruction rate of absorption cycle components.

Fig. 4 shows the exergy destruction rate of Rankine cycle components and Fig. 5 shows the exergy destruction of adsorption refrigeration cycle components. According to Fig. 4, the highest rate of exergy destruction (34%) is related to the desuperheater, which is the cause of the large temperature difference between the two fluids. For this purpose, and to use the recycled heat of this component, an adsorption refrigeration cycle is coupled to the Rankin cycle, which uses the superheater heat to produce cooling in the absorption cycle evaporator. The degree of exergy destruction of the absorption refrigeration cycle components is shown in Fig. 5 which is aligned with the results of other papers [30-50].

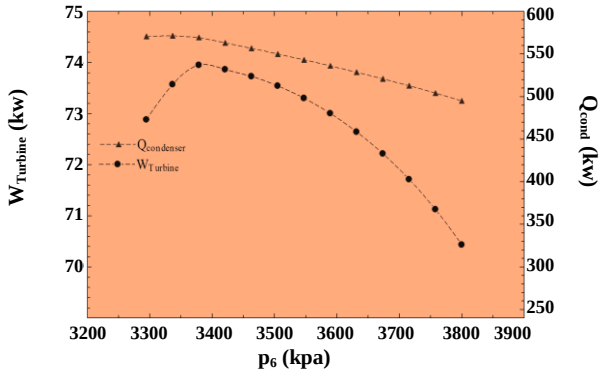

Fig. 6: Turbine power and condenser heat with pressure P6.

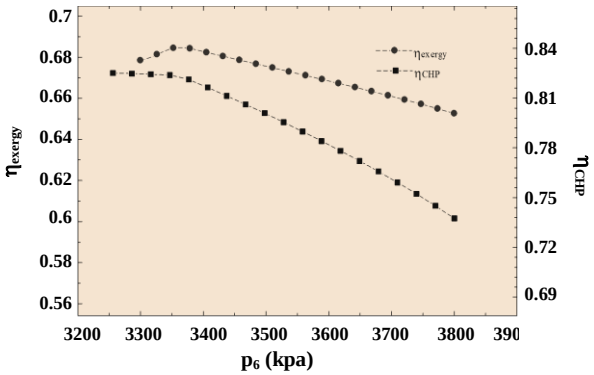

Fig. 7: Energy efficiency and exergy of the system with pressure P6.

According to Fig. 5, the most exergy destruction with 36% is related to the absorber part and then the absorption cycle condenser with 34% is the most exergy destruction.

Parametric analysis

In this paper throttle and turbine outlet pressures are studied. These two parameters are effective on all other parameters of the system. The Upper and lower pressure of a Rankine cycle determines the power output of the system and Both the Turbine inlet and outlet can be considered the most important parameters in designing any Rankine system. The turbine inlet is the throttle pressure which significantly impacts the overall performance and configuration of the system and turbine outlet pressure is effective on the condensing system and turbine sizing [50-60].

To influence the system parameters on system performance, parametric analysis is performed. Fig. 6 shows the changes in turbine output power and condenser heat released in terms of pre-turbine pressure (P6). As the turbine inlet pressure increases, the turbine output power initially increases, and this increase continues to 3436 kPa. After that, with the increasing pressure of the fluid entering the turbine, the production capacity decreases. On the other hand, the amount of heat released in the condenser increases with increasing turbine inlet pressure to 3362 kPa and then decreases. Parametric changes based on Figs. 6-8 have created the optimal point for the turbine output power, system energy, and exergy efficiency, the amount of hydrogen produced and the heat released in the condenser. The existence of an optimal point for the organic Rankin cycle, according to the second equation of Table 4, will optimize the power required for the electrochemical reaction, followed by the current density and the amount of hydrogen produced, because obtaining the optimal turbine inlet pressure point in the Rankin cycle creates the corresponding optimal point in The electrolyzer system and the heat acquired by the water will enter the proton membrane system[60-75].

On the other hand, changes in system parameters will create an optimal state for the system's exergy efficiency and the heat absorbed in the absorption cycle evaporator. With increasing turbine inlet pressure, the amount of exergy efficiency first increases and then decreases. Still, the amount of heat absorbed in the evaporator decreases steadily with increasing turbine inlet pressure, which causes the turbine inlet temperature to decrease and consequently decrease. The enthalpy and heat given to the generator will be the absorption cycle. Therefore, system optimization has led to finding the optimal pressure for the turbine. These changes are shown in Fig. 9.

The results of the effect of turbine outlet pressure on the energy efficiency and exergy of the cogeneration system are shown in Fig. 10. As the output pressure of the turbine increases, the temperature and enthalpy of point 7 will increase, and following the decrease in the production capacity of the turbine, the amount of energy efficiency and exergy will also decrease. On the other hand, as the output pressure of the turbine increases, the amount of heat produced in the superheater increases. To find the optimal point of turbine outlet pressure, changes in turbine outlet pressure with changes in turbine output power and energy and exergy efficiencies have been investigated.

The changes in heat released in the superheater, the turbine generating capacity, the energy efficiency, and the exergy of the system simultaneously are shown in Figs. 10-12.

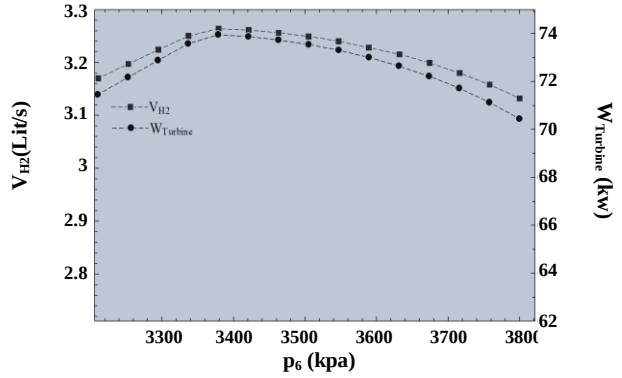

Fig. 8: Hydrogen production and turbine power with pressure P6.

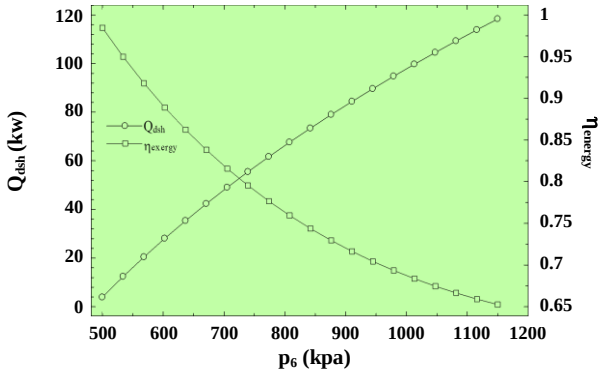

Fig. 11: Superheater heat and exergy efficiency(Pressure P7).

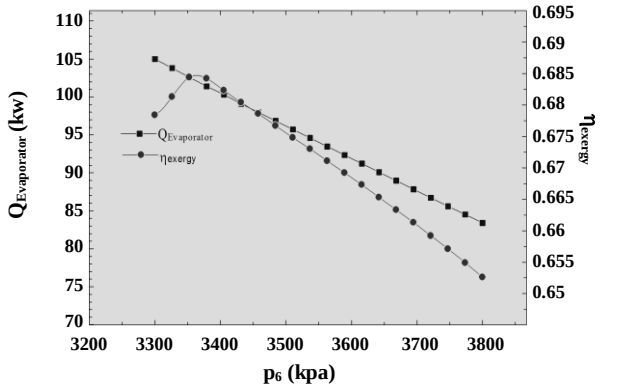

Fig. 9: Evaporator heat and exergy efficiency with pressure P6.

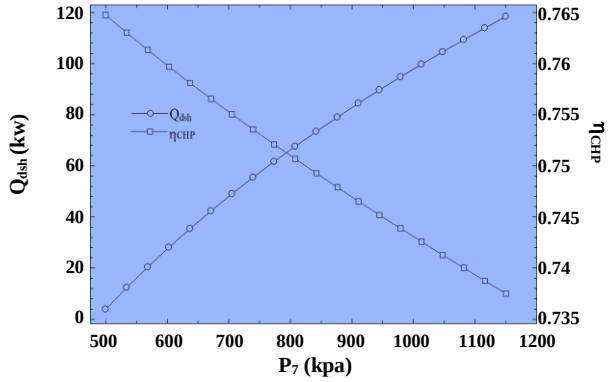

Fig. 12: Superheater heat and system energy efficiency (Pressure P7).

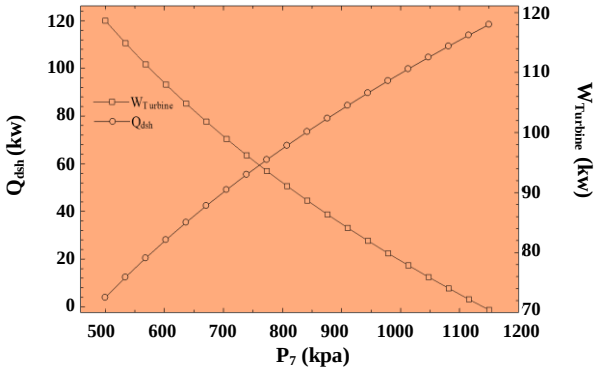

Fig. 10: Superheater heat and P7 pressure output power.

According to the results of Figs. 10, 11, and 12, with increasing turbine outlet pressure, the amount of heat released in the superheater (Q_{dsh}) also increases due to the higher inlet temperature of the superheater, but on the other hand, the amount of turbine work is energy efficiency. And the exergy efficiency of the cogeneration system is reduced. Due to the changes in the system's operating parameters and according to Figs. 10, 11, and 12, the power output, energy efficiency and exergy of the system have an optimal point relative to the turbine output pressure.

Optimization results

The results of the cogeneration system optimization calculations are presented in Table 8. This optimization has been done from three different perspectives. According to the results of Table 8, the performance parameters of the system are different from different perspectives. From the point of view of maximizing the production capacity of the turbine, in this case, the amount of production power, cogeneration efficiency, and the amount of hydrogen produced are equal to 101.2 kW, 0.8229, and 4.239 liters per second, respectively. The constraints and investigation parameters are explained in Table 5. The initial population is set 50 and the generation number is 200.

CONCLUSIONS

In this research, the proposed power, cooling, and hydrogen cogeneration system was thermodynamically analyzed and optimized from three different approaches.

Table 8: Optimal performance of the proposed cycle from three different approaches.

Optimal values	To exergy efficiency	To the efficiency of the cogeneration system	To the power of the turbine
Turbine inlet pressure (kPa)	3362	3366	3436
Turbine outlet pressure (kPa)	725.1	792.1	732.4
Turbine output power (kW)	105.3	99.31	101.3
Cogenerative energy efficiency	0.839	0.833	0.823
Cogenerative exergy efficiency	0.842	0.791	812.0
Hydrogen production (L/s)	4.38	4.17	4.24
Condenser heating (kW)	480.0	660	652.6
Superheater heating (kW)	79.6	91.5	81.8
Heat absorbed in the evaporator (kW)	56.0	64.5	57.6

The main results of the research can be briefly described as below. In summary, the highest amount of exergy destruction in the organic Rankin cycle was obtained for the superheater and in the absorption cycle for the absorber. Also, from the point of view of maximum turbine output power(most optimum state), energy and exergy efficiency and the amount of hydrogen produced in the system were equal to 101.2 kW, 82.3%, 81.0%, and 4.239l/s, respectively.

Received : Oct. 10, 2021 ; Accepted : Jan. 31, 2022

REFERENCES

[1] Zhu J., Hu K., Lu X., Huang X., Liu K., Wu X., A Review of Geothermal Energy Resources, Development, and Applications in China: Current Status and Prospects, *Energy*, **93**: 466-483 (2015).

[2] Alhamid M.I., Daud Y., Surachman A., Sugiyono A., Aditya H.B., Mahlia T.M.I., Potential of Geothermal Energy for Electricity Generation in Indonesia: A Review, *Renewable and Sustainable Energy Reviews*, 53: 733-740 (2016).

[3] Michaelides E.E.S., Future Directions and Cycles for Electricity Production from Geothermal Resources, *Energy Conversion and Management*, **107**: 3-9 (2016).

[4] Wu C., Wang S.S., Li J., Exergoeconomic Analysis and Optimization of a Combined Supercritical Carbon Dioxide Recompression Brayton/Organic Flash Cycle for Nuclear Power Plants, *Energy Conversion and Management*, **171**: 936-952 (2018).

[5] Hsieh J.C., Lee Y.R., Guo T.R., Liu L.W., Cheng P.Y., Wang, C.C., A co-axial Multi-Tube Heat Exchanger Applicable for a Geothermal ORC Power Plant, *Energy Procedia*, **61**: 874-877 (2014).

[6] Astolfi M., Romano M.C., Bombarda P., Macchi E., Binary ORC (Organic Rankine Cycles) Power Plants for the Exploitation of Medium–Low Temperature Geothermal Sources–Part B: Techno-Economic Optimization, *Energy*, **66**: 435-446 (2014).

[7] Zhai H., Shi L., An Q., Influence of Working Fluid Properties on System Performance and Screen Evaluation Indicators for Geothermal ORC (Organic Rankine Cycle) System, *Energy*, **74**, 2-11(2014).

[8] Orhan M. F., Babu B. S., Investigation of an Integrated Hydrogen Production System Based on Nuclear and Renewable Energy Sources: Comparative Evaluation of Hydrogen Production Options with a Regenerative Fuel Cell System, *Energy*, **88**: 801-820 (2015).

[9] Zhong J., Stevens D.K., Hansen C.L., Optimization of Anaerobic Hydrogen and Methane Production from Dairy Processing Waste Using a Two-Stage Digestion in Induced Bed Reactors (IBR), *International Journal of Hydrogen Energy*, **40(45)**: 15470-15476 (2015).

[10] Monfort O., Pop L.C., Sfaelou S., Plecenik T., Roch T., Dracopoulos V., Stathatos E., Plesch G., Lianos P., Photoelectrocatalytic Hydrogen Production by Water Splitting Using $BiVO_4$ Photoanodes, *Chemical Engineering Journal*, **286**: 91-97 (2016).

[11] Dincer I., Green Methods for Hydrogen Production, *International Journal of Hydrogen Energy*, **37(2)**: 1954-1971 (2012).

[12] Caliskan H., Dincer I., Hepbasli A., Energy, Exergy and Sustainability Analyses of Hybrid Renewable Energy Based Hydrogen and Electricity Production and Storage Systems: Modeling and Case Study, *Applied Thermal Engineering*, **61(2)**: 784-798 (2013).

[13] Pham A.T., Baba T., Shudo T., Efficient Hydrogen Production from Aqueous Methanol in a PEM Electrolyzer with Porous Metal Flow Field: Influence of Change in Grain Diameter and Material of Porous Metal Flow Field, *International Journal of Hydrogen Energy*, **38(24)**: 9945-9953 (2013).

[14] Ratlamwala T., Dincer I., Comparative Efficiency Assessment of Novel Multi-Flash Integrated Geothermal Systems for Power and Hydrogen Production, *Applied Thermal Engineering*, **48**: 359-66, (2012).

[15] Cao Y., Haghghi M.A., Shamsaiee M., Athari H., Ghaemi M, Rosen M.A., Evaluation and Optimization of a Novel Geothermal-Driven Hydrogen Production System Using an Electrolyser Fed by a Two-Stage Organic Rankine Cycle with Different Working Fluids, *Journal of Energy Storage*, **32**:101766 (2020).

[16] Atalay H., Comparative Assessment of Solar and Heat Pump Dryers with Regards to Exergy and Exergoeconomic Performance, *Energy*, **189**: 116180 (2019).

[17] Norouzi N., Fani M., Talebi S., Exergetic Design and Analysis of a Nuclear SMR Reactor Tetrageneration (Combined Water, Heat, Power, and Chemicals) with Designed PCM Energy Storage and a CO_2 Gas Turbine Inner Cycle, *Nuclear Engineering and Technology*, **53(2)**: 677-687 (2021).

[18] Yuksel Y.E., Ozturk M., Thermodynamic and Thermoeconomic Analyses of a Geothermal Energy Based Integrated System for Hydrogen Production, *International Journal of Hydrogen Energy*, **42(4)**: 2530-2546 (2017).

[19] Norouzi N., Talebi S., Fani M., Khajehpour H., Exergy and Exergoeconomic Analysis of Hydrogen and Power Cogeneration Using an HTR Plant, *Nuclear Engineering and Technology*, **53(8)**: 2753-2760 (2021).

[20] Balta M.T., Dincer I., Hepbasli A., Exergoeconomic Analysis of a Hybrid Copper–Chlorine Cycle Driven by Geothermal Energy for Hydrogen Production, *International Journal of Hydrogen Energy*, **36(17)**: 11300-11308 (2011).

[21] Cai Q., Adjiman C.S., Brandon N.P., Optimal Control Strategies for Hydrogen Production when Coupling Solid Oxide Electrolysers with Intermittent Renewable Energies, *Journal of Power Sources*, **268**: 212-224 (2014).

[22] Ouali S., Chader S., Belhamel M., Benziada M., The Exploitation of Hydrogen Sulfide for Hydrogen Production in Geothermal Areas, *International Journal of Hydrogen Energy*, **36(6)**: 4103-4109 (2011).

[23] Mahmoud M., Ramadan M., Naher S., Pullen K., Abdelkareem M.A., Olabi A.G. A Review of Geothermal Energy-Driven Hydrogen Production Systems, *Thermal Science and Engineering Progress*, **22**: 100854 (2021).

[24] Parham K, Assadi M., A Parametric Performance Analysis of a Novel Geothermal Based Cogeneration System, In "Sustainable Energy Technology and Policies", pp. 167-182, Springer, Singapore. (2018)

[25] Han J., Wang X., Xu J., Yi N., Talesh S.S., Thermodynamic Analysis and Optimization of an Innovative Geothermal-Based Organic Rankine Cycle Using Zeotropic Mixtures for Power and Hydrogen Production, *International Journal of Hydrogen Energy*, **45(15)**:8282-8299 (2020).

[26] Yuksel Y.E., Ozturk M., Dincer I. Energetic and Exergetic Performance Evaluations of a Geothermal Power Plant Based Integrated System for Hydrogen Production, *International Journal of Hydrogen Energy*, **43(1)**: 78-90 (2018).

[27] Cao Y., Dhahad H.A., Togun H., Hussen H.M., Rashid T.A., Anqi A.E., Farouk N., Issakhov A. Exergetic and Financial Parametric Analyses and Multi-Objective Optimization of a Novel Geothermal-Driven Cogeneration Plant; Adopting a Modified Dual Binary Technique, *Sustainable Energy Technologies and Assessments*, **48**:101442 (2021).

[28] Cao L., Lou J., Wang J., Dai Y., Exergy Analysis and Optimization of a Combined Cooling and Power System Driven by Geothermal Energy for Ice-Making and Hydrogen Production, *Energy Conversion and Management*, **174**: 886-896 (2018).

[29] Yilmaz C., Koyuncu I., Alcin M., Tuna M., Artificial Neural Networks Based Thermodynamic and Economic Analysis of a Hydrogen Production System Assisted by Geothermal Energy on Field Programmable Gate Array, *International Journal of Hydrogen Energy*, **44(33)**:17443-17459 (2019).

[30] Talebi S., Norouzi N., Entropy and Exergy Analysis and Optimization of the VVER Nuclear Power Plant with a Capacity of 1000 MW Using the Firefly Optimization Algorithm, *Nuclear Engineering and Technology*, **52(12)**: 2928-2938 (2020).

[31] Norouzi N., 4E Analysis of a Fuel Cell and Gas Turbine Hybrid Energy System, *Biointerface Res. Appl. Chem.*, **11(1)**: 7568-7579 (2021).

[32] Norouzi N., Talebi S., Exergy and Energy Analysis of Effective Utilization of Carbon Dioxide in the Gas-To-Methanol Process, *Iranian Journal of Hydrogen & Fuel Cell*, **7(1)**: 13-31 (2020).

[33] Norouzi N., 4E Analysis and Design of a Combined Cycle with a Geothermal Condensing System in Iranian Moghan Diesel Power Plant, *International Journal of Air-Conditioning and Refrigeration*, **28(03)**: 2050022 (2020).

[34] Algieri A., Morrone P., Energetic Analysis of Biomass-Fired ORC Systems for Micro-Scale Combined Heat and Power (CHP) Generation. A Possible Application to the Italian Residential Sector, Applied Thermal Engineering, **71(2)**: 751-759 (2014).

[35] Norouzi N., Hosseinpour M., Talebi S., Fani M., A 4E Analysis of Renewable Formic Acid Synthesis from The Electrochemical Reduction of Carbon Dioxide and Water: Studying Impacts of the Anolyte Material on the Performance of the Process, *Journal of Cleaner Production*, **293**: 126149 (2021).

[36] Wang J., Yan Z., Wang M., Ma S., Dai Y., Thermodynamic Analysis and Optimization of an (Organic Rankine Cycle) ORC Using Low Grade Heat Source, *Energy*, **49**: 356-365 (2013).

[37] Leveni M., Manfrida G., Cozzolino R., Mendecka B., Energy and Exergy Analysis of Cold and Power Production from the Geothermal Reservoir of Torre Alfina, *Energy*, **180**: 807-818 (2019).

[38] Zha T.H., Castillo, O., Jahanshahi H., Yusuf A., Alassafi M.O., Alsaadi F.E., Chu Y.M., A Fuzzy-Based Strategy to Suppress the Novel Coronavirus (2019-NCOV) Massive Outbreak, *Applied and Computational Mathematics*, **20(1)**:160-176 (2021).

[39] Zhao T., Wang M., Chu Y., On the Bounds of the Perimeter of an Ellipse, *Acta Mathematica Scientia*, **42(2)**: 491-501(2022).

[40] Zhao T.H., Wang M.K., Hai G.J., Chu Y.M., Landen Inequalities for Gaussian Hypergeometric Function. Revista de la Real Academia de Ciencias Exactas, *Físicas y Naturales. Serie A. Matemáticas*, **116(1)**: 1-23 (2022).

[41] Nazeer M., Hussain F., Khan M.I., El-Zahar E.R., Chu Y.M., Malik M.Y., Theoretical study of MHD Electro-Osmotically Flow of Third-Grade Fluid in Micro Channel, *Applied Mathematics and Computation*, **420**: 126868 (2022).

[42] Chu Y.M., Shankaralingappa B.M., Gireesha B.J., Alzahrani F., Khan M.I., Khan S.U., Combined Impact of Cattaneo-Christov Double Diffusion and Radiative Heat Flux on Bio-Convective Flow of Maxwell Liquid Configured by a Stretched Nano-Material Surface, *Applied Mathematics and Computation*, **419**: 126883 (2022).

[43] Zhao T.H., Khan M.I., Chu Y.M., Artificial Neural Networking (ANN) Analysis for Heat and Entropy Generation in Flow of Non- Newtonian Fluid Between Two Rotating Disks, *Mathematical Methods in the Applied Sciences*, 1– 19 (2021).

[44] Iqbal M.A., Wang Y., Miah M.M., Osman M.S., Study on Date–Jimbo–Kashiwara–Miwa Equation with Conformable Derivative Dependent on Time Parameter to Find the Exact Dynamic Wave Solutions, *Fractal and Fractional*, **6(1)**: 4 (2021).

[45] Zhao T.H., He Z.Y., Chu Y.M., Sharp Bounds for The Weighted Hölder Mean of The Zero-Balanced Generalized Complete Elliptic Integrals, *Computational Methods and Function Theory*, **21(3)**: 413-426 (2021).

[46] Zhao T.H., Wang M.K., Chu Y.M., Concavity and Bounds Involving Generalized Elliptic Integral of the First Kind, *J. Math. Inequal.*, **15(2)**: 701-724 (2021).

[47] Chu H.H., Zhao T.H., Chu Y.M., Sharp Bounds for the Toader Mean of Order 3 in Terms of Arithmetic, Quadratic and Contraharmonic Means, *Mathematica Slovaca*, **70(5)**:1097-1112 (2020).

[48] Zhao T.H., He Z.Y., Chu Y.M., On Some Refinements for Inequalities Involving Zero-Balanced Hypergeometric Function, *AIMS Math*, **5(6)**: 6479-6495(2020).

[49] Zhao T.H., Wang M.K., Chu, Y.M., A Sharp Double Inequality Involving Generalized Complete Elliptic Integral of the First Kind, *AIMS Math*, **5(5)**: 4512-4528 (2020).

[50] Zhao T.H., Shi L., Chu Y.M., Convexity and Concavity of the Modified Bessel Functions of the First Kind with Respect to Hölder Means. Revista de la Real Academia de Ciencias Exactas, Físicas y Naturales, *Serie A. Matemáticas*, **114(2)**: 1-14 (2020).

[51] Zhao T.H., Zhou B.C., Wang M.K., Chu Y.M., On Approximating the Quasi-Arithmetic Mean, *Journal of Inequalities and Applications*, **2019(1)**: 1-12 (2019).

[52] Zhao T.H., Wang M.K., Zhang W., Chu Y.M., Quadratic Transformation Inequalities for Gaussian Hypergeometric Function, *Journal of Inequalities and Applications*, **2018(1)**: 1-15 (2018).

[53] Chu Y.M., Zhao T.H., Concavity of the Error Function with Respect to Hölder Means, *Math. Inequal. Appl*, **19(2)**: 589-595 (2016).

[54] Zhao T.H., Shen Z.H., Chu Y.M., Sharp Power Mean Bounds for the Lemniscate Type Means, *Revista de la Real Academia de Ciencias Exactas, Físicas y Naturales. Serie A. Matemáticas*, **115(4)**: 1-16 (2021).

[55] Song Y.Q., Zhao T.H., Chu Y.M., Zhang X.H., Optimal evaluation of a Toader-Type Mean by Power Mean, *Journal of Inequalities and Applications*, **2015(1)**: 1-12 (2015).

[56] Chu Y.M., Zhao T.H., Convexity and Concavity of the Complete Elliptic Integrals with Respect to Lehmer Mean, *Journal of Inequalities and Applications*, **2015(1)**: 1-6 (2015).

[57] Zhao T.H., Yang Z.H., Chu Y.M., Monotonicity Properties of a Function Involving the Psi Function with Applications, *Journal of Inequalities and Applications*, **2015(1)**: 1-10 (2015).

[58] Chu Y.M., Wang H., Zhao T.H., Sharp Bounds for the Neuman Mean in Terms of the Quadratic and Second Seiffert Means, *Journal of Inequalities and Applications*, **2014(1)**: 1-14 (2014).

[59] Sun H., Zhao T.H., Chu Y.M., Liu B.Y., A Note on the Neuman-Sándor Mean, *J. Math. Inequal*, **8(2)**: 287-297 (2014).

[60] Chu Y.M., Zhao T.H., Liu B.Y., Optimal Bounds for Neuman-Sándor Mean in Terms of the Convex Combination of Logarithmic and Quadratic or Contra-Harmonic Means, *J. Math. Inequal*, **8(2)**: 201-217 (2014).

[61] Chu Y.M., Zhao T.H., Song Y.Q., Sharp Bounds For Neuman-Sándor Mean in Terms of the Convex Combination of Quadratic and First Seiffert Means, *Acta Mathematica Scientia*, **34(3)**: 797-806 (2014).

[62] Zhao T.H., Chu Y.M., Jiang Y.L., Li Y.M., Best Possible Bounds for Neuman-Sándor Mean by the Identric, Quadratic and Contraharmonic Means, In *Abstract and Applied Analysis* (Vol. 2013). Hindawi (2013).

[63] Zhao T.H., Chu Y.M., Liu B.Y., Optimal Bounds for Neuman-Sándor Mean in Terms of the Convex Combinations of Harmonic, Geometric, Quadratic, and Contraharmonic Means, *Abstract and Applied Analysis* (Vol. 2012). (2012). [Hindawi]

[64] Wang M.K., Hong M.Y., Xu Y.F., Shen Z.H., Chu Y.M., Inequalities for Generalized Trigonometric and Hyperbolic Functions with one Parameter, *J. Math. Inequal*, **14(1)**: 1-21 (2020).

[65] Xu H.Z., Qian W.M., Chu Y.M., Sharp Bounds for the Lemniscatic Mean by the One-Parameter Geometric and Quadratic Means, *Rev. R. Acad. Cienc. Exactas Fís. Nat. Ser. A Mat. RACSAM*, **116(1)**: 15 (2022).

[66] Karthikeyan K., Karthikeyan P., Baskonus H.M., Venkatachalam K., Chu Y.M., Almost Sectorial Operators on Ψ- Hilfer Derivative Fractional Impulsive Integro- Differential Equations, *Mathematical Methods in the Applied Sciences* (2021).

[67] Chu Y.M., Nazir U., Sohail M., Selim M.M., Lee J.R., Enhancement in Thermal Energy and Solute Particles Using Hybrid Nanoparticles by Engaging Activation Energy and Chemical Reaction over a Parabolic Surface Via Finite Element Approach, *Fractal and Fractional*, **5(3)**: 119 (2021).

[68] Rashid S., Sultana S., Karaca Y., Khalid A., Chu Y.M., Some Further Extensions Considering Discrete Proportional Fractional Operators, *Fractals*, **30(1)**: 2240026(2022).

[69] Zhao T.H., Qian W.M., Chu, Y.M., Sharp Power Mean Bounds for the Tangent and Hyperbolic Sine Means, *Journal of Mathematical Inequalities*, **15(4)**: 1459-1472 (2021).

[70] Zhao T.H., Qian W.M., Chu Y.M., On Approximating the Arc Lemniscate Functions, *Indian Journal of Pure and Applied Mathematics*, 1-14 (2021).

[71] Hajiseyedazizi S.N., Samei M.E., Alzabut J., Chu Y.M., On Multi-Step Methods for Singular Fractional Q-Integro-Differential Equations, *Open Mathematics*, **19(1)**: 1378-1405 (2021).

[72] He Z.Y., Abbes A., Jahanshahi H., Alotaibi N.D., Wang Y., Fractional-Order Discrete-Time SIR Epidemic Model with Vaccination: Chaos and Complexity, *Mathematics*, **10(2)**:165 (2022).

[73] Jin F., Qian Z.S., Chu Y.M., ur Rahman M., On Nonlinear Evolution Model for Drinking Behavior under Caputo-Fabrizio Derivative, *Journal of Applied Analysis & Computation*, **12(2):** 790-806 (2022).

[74] Rashid S., Abouelmagd E.I., Khalid A., Farooq F.B., Chu Y.M., Some Recent Developments on Dynamical $\hbar$ -Discrete Fractional Type Inequalities in the Frame of Nonsingular and Nonlocal Kernels, *Fractals*, **30(2)**: 15 (2021).

[75] Wang F., Khan M.N., Ahmad I., Ahmad H., Abu-Zinadah H., Chu Y.M., Numerical Solution of Traveling Waves in Chemical Kinetics: Time-Fractional Fishers Equations, *Fractals*, 2240051 (2022).